ACS OMEGA

http://pubs.acs.org/journal/acsodf

Article

Three-Dimensional, MultiScale, and Interconnected Trabecular Bone Mimic Porous Tantalum Scaffold for Bone Tissue Engineering

Xiaoyu Wang, Zhenglin Zhu, Haozuo Xiao, Changqi Luo, Xiaoji Luo, Furong Lv, Junyi Liao,* and Wei Huang*

Cite This: *ACS Omega* 2020, 5, 22520−22528

Read Online

ACCESS | Metrics & More | Article Recommendations

ABSTRACT: To investigate the biocompatibility and bone ingrowth properties of a novel trabecular bone mimic porous tantalum scaffold which holds potential for bone tissue engineering, a novel three-dimensional, multiscale interconnected porous tantalum scaffold was designed and manufactured. The morphology of the novel scaffold was observed with the use of scanning electron microscopy (SEM) and industrial computerized tomography. Mesenchymal stem cells (MSCs) were cultured with novel porous tantalum powder, SEM was carried out for the observation of cell morphology and adhesion, and cytotoxicity was evaluated by the MTT assay. Canine femoral shaft bone defect models were established, and novel porous tantalum rods were used to repair the bone defect. Repair effects and bone integration were evaluated by hard tissue slice examination and push-out tests at the indicated time. We found that the novel porous tantalum scaffold is a trabecular bone mimic, having the characteristics of being three-dimensional, multiscaled, and interconnected. The MSCs adhered to the surface of tantalum and proliferated with time, the tantalum extract did not have a cytotoxic effect on MSCs. In the bone defect model, porous tantalum rods integrated tightly with the host bone, and new bone formation was found on the scaffold-host bone interface both 3 and 6 months after the implantation. Favorable bone ingrowth was observed in the center of the tantalum rod. The push-out test showed that the strength needed to push out the tantalum rod is comparable for both 3 and 6 months when compared with the normal femoral shaft bone tissue. These findings suggested that the novel trabecular bone mimic porous tantalum scaffold is biocompatible and osteoinductive, which holds potential for bone tissue engineering application.

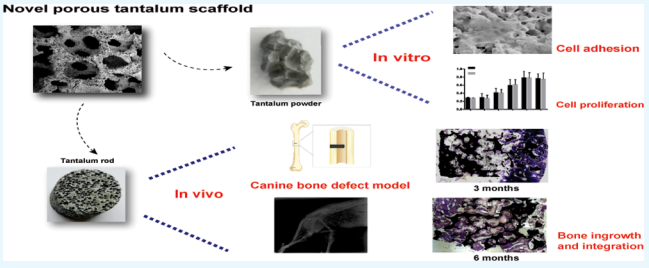

INTRODUCTION

Trauma, tumor resection, bone infection, and regenerative disorder-caused bone defects are a challenge to the medical fraternity.[1−4] Autograft and allograft transplantations are the common methods applied by surgeons to treat bone defects; however, limited bone sources and immunological reactions are still a cause for worry.[4−6] Therefore, surgeons have long been interested in taking advantage of the properties of various metals for the reconstruction of bone defects.[7−11] In recent years, titanium and its alloys have been widely utilized to produce orthopedic implants such as total hip arthroplasty (THA) and total knee arthroplasty (TKA) prostheses, spinal fusion cage, and bone plate and so forth.[7,12] Nevertheless, high elastic modulus, low porosity, and low surface friction coefficient and of titanium blocked their clinical applications for bone defect.[7,13,14] Therefore, a material with higher porosity, higher surface friction coefficient, and lower elastic modulus compared with titanium holds potential for bone tissue engineering.

Tantalum is a bioinert metal which holds the characteristic of anticorrosion in vivo compared with other metal materials.[7,15,16] As a bone repair material, porous tantalum was applied to arthroplasty, dental implants, spinal fusion surgery, foot and ankle surgery, necrosis of femoral head treatment, and so forth.[7,9,14,17−21] Its high porosity, high surface friction coefficient, favorable compatibility, and proper elastic modulus approximate to cancellous bone make it a promising material for bone tissue engineering,[7,22] while an ideal material for bone tissue engineering should be trabecular bone mimic, osteoinductive, and hold the capacity for bone ingrowth,[8,13,23,24] so we developed a novel trabecula bone mimic porous tantalum, which is three-dimensional, multiscale, and interconnected. Compared with the porous tantalum manufactured by Zimmer Corporation (Warsaw, IN, USA),[17,20−22,25] our novel porous tantalum holds a wider

Received: June 29, 2020
Accepted: August 10, 2020
Published: August 25, 2020

https://dx.doi.org/10.1021/acsomega.0c03127
ACS Omega 2020, 5, 22520−22528

range of porosity from 60 to 80% (Zimmer, 75−85%), wider range of pore diameter from 200 to 500 μm (Zimmer, 400−600 μm), and lower elastic modulus range from 0.5 to 4.0 GPa (Zimmer, 2.5−3.9 GPa). These differences make the novel porous tantalum property closer to the cancellous bone.

In this study, we investigated physical properties, biocompatibility, cytotoxicity, and osteoinductive characteristics of the novel porous tantalum scaffold by in vitro and/or in vivo tests, the results indicated that the novel porous tantalum has potential for bone tissue engineering application.

RESULTS

Structural Characterization of Novel Porous Tantalum Scaffold. The biomechanical indexes are shown in Table 1. To understand the tridimensional structure and microstructure of the novel porous tantalum scaffold, the porous tantalum was subjected to scanning electron microscopy (SEM) analysis. As shown in Figure 1, the material was three-dimensional and in a honeycomb pattern with pore diameters ranging from 200 to 500 μm (Figure 1A); meanwhile, the material was interconnected with microscopic pores with diameters ranging from 1 to 10 μm (Figure 1A−C). The honeycomb structure was also confirmed by industrial computerized tomography (CT) analysis. As shown in Figure 1C, the longitudinal and transverse images manifested that the material consisted of mesh shape pores in different sizes. Macroscopic images of porous tantalum powders and rods revealed that the material was gray and smooth, and pinpoint-sized pores in different diameters distributed on the surfaces. These results suggested that the novel porous tantalum scaffold is trabecular bone mimic, having the characteristic of being three-dimensional, multiscaled, and interconnected.

Table 1. Physical Parameters of Novel Porous Tantalum

parameters	range
density (g/cm^3)	3.5−7.0
porosity (%)	60−80%
pore diameter (μm)	200−500
microcosmic pore diameter (μm)	1−10
elasticity modulus (GPa)	0.5−4.0
yield strength (MPa)	75−120
ultimate tensile strength (MPa)	110−210
tensile strength (MPa)	80−120

Cell Growth on the Novel Porous Tantalum Scaffold. Next, biocompatibility of the novel porous tantalum scaffold was examined with the use of mesenchymal stem cells (MSCs). UC-MSC cells were seeded on the porous tantalum scaffold and incubated in complete Dulbecco modified Eagle medium (DMEM) and subjected to the SEM test at the indicated time points. On day 3, we found the cells survived and were attached stably on the porous tantalum scaffold (Figure 2Aa). On the higher magnification, we found that the cell was stretched out and cytoplasm extended outside to form protrusions (Figure 2Ab). On day 5, the cell number increased compared with on day 3, which indicated the proliferation of the cells. The cells attached and connected with each other to form a layer on the surface of the porous tantalum scaffold (Figure 2Ac). On the higher magnification (Figure 2Ad), we detected that the cells had grown into the inner side of the material and formed protrusions connected with each other. The results demonstrated the porous tantalum scaffold was biocompatible and suitable for cell proliferation.

Cytotoxicity of Porous Tantalum Extract. To monitor the influence of the porous tantalum extract on the proliferation of UC-MSCs, MTT assay was used. Absorbance values showed that from day 1 to day 6, the growth rate of the UC-MSCs in the control group accelerated gradually, ultimately entering a stable phase. Compared with the control group, the experiment group showed the same trend, and no statistically significance difference ($p > 0.05$) of the absorbance value was found on each day (Figure 2B). These results indicated that the porous tantalum extract was not cytotoxic to UC-MSCs, achieving the basic requirement of implant materials.

Construction of Canine Femoral Shaft Bone Defect Models and Implantation of the Porous Tantalum Rod. To mimic the defects of long bone shaft, canine femoral shaft bone defect models were constructed. Briefly, a diameter of ∼4

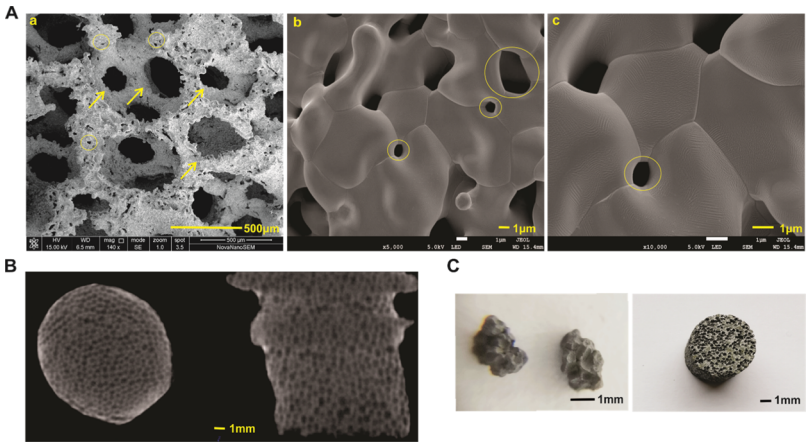

Figure 1. Physical properties and morphology of porous tantalum (photograph courtesy of "Chongqing Runze Pharmaceutical Co., Ltd". Copyright 2020). (A) SEM micrographs of novel porous tantalum scaffold. Honeycomb pattern with pore diameters range from 200 to 500 μm in 400 magnification (a, scale bar = 500 μm). Microscopic pores (range from 1 to 10 μm) in 5000 magnification (b, scale bar = 1 μm) and 10,000 magnification (c, scale bar = 1 μm). Arrows indicate the pores in the millimeter level, circles indicate the interconnected microscopic pore in the micron level. (B) Industrial CT images for the tantalum rod, scale bar = 1 μm. (C) Morphology of novel porous tantalum powder and tantalum rod, scale bar = 1 mm.

https://dx.doi.org/10.1021/acsomega.0c03127
ACS Omega 2020, 5, 22520−22528

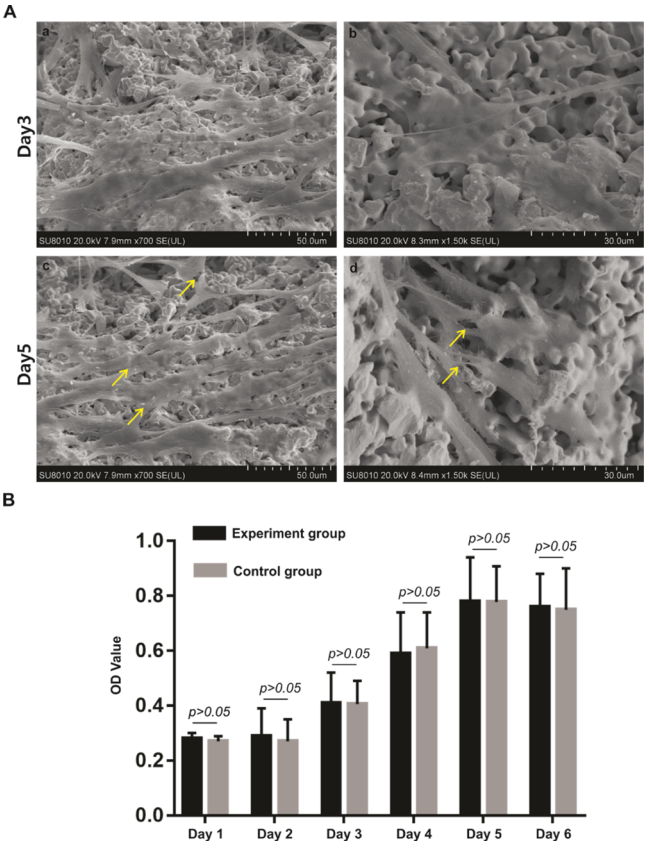

Figure 2. Cell growth on a novel porous tantalum scaffold and cytotoxicity evaluation of porous tantalum scaffold. (A) SEM micrographs of UC-MSCs on the porous tantalum scaffold at different time points. UC-MSCs on the porous tantalum scaffold on day 3 (a, scale bar = 50 μm, b, scale bar = 30 μm). UC-MSCs on the porous tantalum scaffold on day 5 (a, scale bar = 50 μm, b, scale bar = 30 μm). (B) Cytotoxicity evaluation of the porous tantalum extract. MTT assay were utilized to evaluate the cell proliferation of UC-MSCs cultured in the tantalum extract and UC-MSCs cultured in complete DMEM were used as the control. Cell proliferation did not statistically differ between the groups with extended cultivation time.

mm of the whole cortex bone defect in the midpiece of the femur shaft was constructed. Then, a porous tantalum rod with a diameter of 4 mm and 8 mm in height was embedded in the bone along with the defect, which was as close as possible to the tunnel host bone, the porous tantalum rod was extended to the middle of the bone marrow cavity (Figure 3Aa). Each animal was implanted two porous tantalum rods on the same side, X-ray was taken 1 month after the operation to confirm that the tantalum rods were in the femur shaft and without a peri-implant fracture (Figure 3Ab). 3 and 6 months after the implantation, the tantalum rods were taken out, the specimens are listed in Figure 3B. The surgical sites exhibited no swelling, bleeding, or oozing, and no implant loss was observed. The morphology of the specimens showed that the tantalum rods were surrounded by the host bone; what was interesting, new bone formation in the bone marrow cavity side was seen in 3 months (Figure 3Bb), and the tantalum rod was connected with the opposite bone cortex in 6 months (Figure 3Bd). Taking these results together, we successfully constructed the canine femoral bone defect model and implanted porous tantalum rods; favorable bone ingrowth was observed by morphology analysis of the specimens.

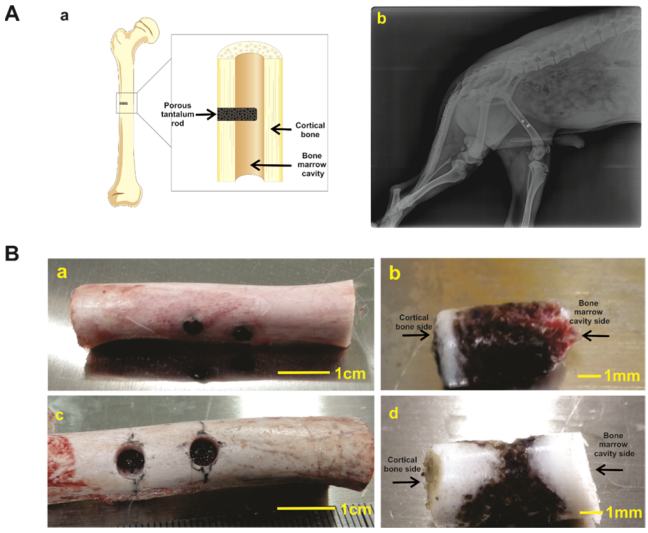

Figure 3. Construction of canine femoral shaft bone defect models and implantation of porous tantalum rod. (A) Graphical diagram for the construction and implantation of porous tantalum rod at canine's midpiece of the femur shaft (a). X-ray image of 1 month after the implantation (b). (B) Retrieved femoral shaft samples at 3 month (a, scale bar = 1 cm) and 6 month (c, scale bar = 1 cm), and retrieved tantalum rod-bone samples at 3 month (b, scale bar = 1 mm) and 6 month (d, scale bar = 1 mm).

Bone Ingrowth and New Bone Formation by Histological Assessment. To further analyze the bone ingrowth and new bone formation of the porous tantalum and host bone interfaces, we took advantage to utilize hard tissue slicing and staining. A merged panoramic version and distinct-separated images by methylene blue and Van Gieson (VG) staining are listed in Figure 4 and 5. For 3 month specimens, no gap between the tantalum scaffold and the host bone was observed in the cortical bone side of the porous tantalum rod, and the porous tantalum and the host bone interfaces were in close contact with each other (Figures 4A and 5A). New trabecular bone was found in the bone marrow cavity side of the porous tantalum (Figures 4Aa–c and 5Aa–c), and bone ingrowth was found in the cortical bone side of the porous tantalum rod (Figures 4Ad and 5Ad). As for 6 month specimens, no gap between the tantalum scaffold and the host bone was observed in the cortical bone side of the porous tantalum rod, and the porous tantalum and the host bone interfaces were in close contact with each other (Figures 4B and 5B). More new trabecular bone was formed and almost filled the porous tantalum pore in the bone marrow cavity side of the porous tantalum (Figures 4Ba–c and 5Ba-c) compared with the 3 month specimens. More bone ingrowth was found in the cortical bone side of the porous tantalum rod compared with the 3 month specimens (Figures 4Bd and 5Bd). Quantitative analysis of new bone formation in 3 and 6 months is shown in Figure 5C. Taking these results together, we identified that the tantalum scaffold and the host bone interfaces integrated with each other in the cortical side of the porous tantalum rod, and a new trabecular bone filled the pore of the material in the bone marrow cavity side of the porous tantalum rod. In other words, the porous tantalum rod possessed the property of bone induction and worked as a good scaffold for bone ingrowth.

Bone Integration of the Porous Tantalum and Host Bone. To confirm the bone integration and determination of

https://dx.doi.org/10.1021/acsomega.0c03127
ACS Omega 2020, 5, 22520−22528

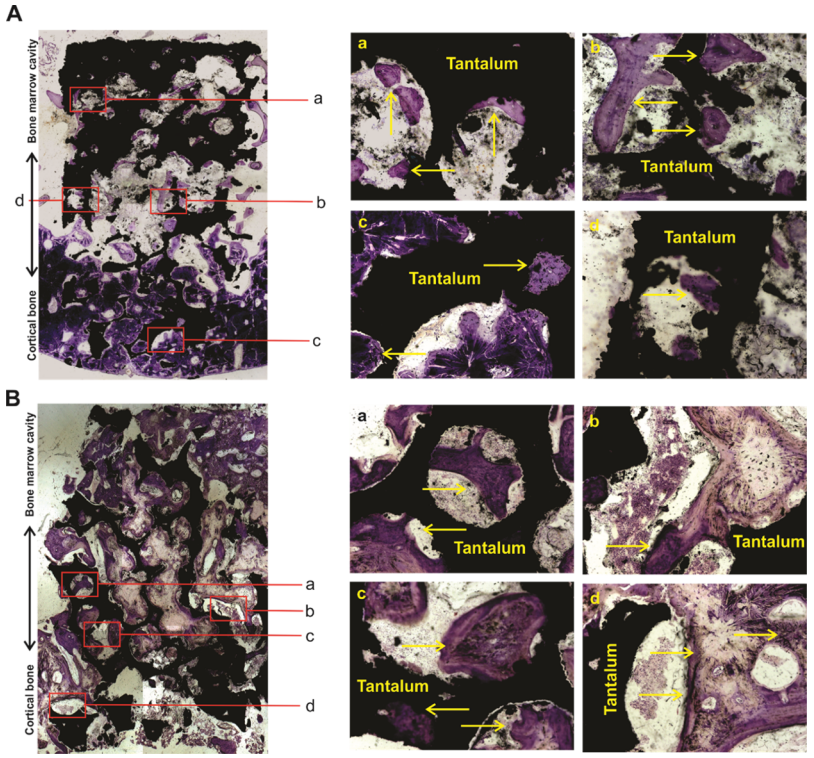

Figure 4. Methylene blue staining for retrieved tantalum rod-bone samples. (A) Methylene blue staining for retrieved tantalum rod-bone samples at 3 months after the implantation. A merged panoramic version in the left panel and distinct-separated images (a−d) are listed in the right panel, arrows indicated the new bone and tantalum rod interfaces. (B) Methylene blue staining for retrieved tantalum rod-bone samples at 6 months after the implantation. A merged panoramic version in the left panel and distinct-separated images (a−d) are listed in the right panel, arrows indicated the new bone and tantalum rod interfaces.

the interfacial bond strength of the tantalum rod and the host bone, the mechanical push-out test was used. The machine is shown in Figure 6A. As shown in Figure 6B, compared with the normal bone, there was no statistically significant difference in strength for pushing the porous tantalum rod out either in the 3 month or 6 month specimens. What was interesting, the strength for pushing porous tantalum rod out in 3 month specimens was not statistically smaller than that in the 6 month specimens. The load-deformation curves are shown in Figure 6C. According to the mode of failure, normal bone was used for the reference of maximum strength, and the two of the 6 month specimens were pushed out by breakage of the host bone. As we found even in the 3 month's specimens, the power for pushing the porous tantalum out from the host bone was comparative with the normal femoral bone, so there is no significant difference among the normal bone, the 3, and 6 month specimens for the push-out test. These results indicated the bone integration of the porous tantalum material and the host bone.

DISCUSSION

Bone defects or nonunion fractures induced by trauma, regenerative disorders, bone tumor, and infection are challenging in treatment for surgeons.[1−4] Although abundant efforts have been devoted to develop bone mimic materials, ideal scaffolds which are osteoinductive, biocompatible, and induce effective bone in-growth at the repair sites are still lacking.[3,10,11,26,27]

In the present study, we manufactured a novel trabecular bone mimic porous tantalum scaffold, which is three-dimensional, multiscaled and interconnected porous material. The structural features were identified by SEM and industrial CT assays. To the best of our knowledge, the porosity, pore diameter, and elastic modulus are closer to cancellous bone compared with porous tantalum produced by Zimmer Corporation.[15−18] Our further canine femoral shaft bone defect models verified that the porous tantalum scaffold is biocompatible and osteoinductive, the integration of the tantalum scaffold and the host bone was also confirmed by mechanical tests. Thus, the novel porous tantalum scaffold holds great potential for further application in bone tissue engineering.

A higher tridimensional surface area was proved to promote cell adhesion, cell growth, and oxygen and nutrition transport.[11,28] In the present study, the tridimensional geometric scaffold structure and interconnected honeycomb-like porous tantalum scaffold material could provide a large internal surface area, and facilitated cell−scaffold interaction in a three-dimensional environment. Except trabecular bone are interconnected physiologically, it was reported that interconnectivity in favor of neovascularization, which maintains sustained bone development and ingrowth, promotes higher volume of host bone and material interaction and offers load transfer along the bone-implant interface.[25,29,30] The novel porous tantalum scaffold featured with interconnected micron pores (Figure 1A), which contributed to the new bone ingrowth and material host bone integration.

The elastic modulus of tantalum is comparative with other metal materials; however, elastic modulus of porous tantalum is much lower, which makes tantalum holds potential to be manufactured as cancellous bone mimic scaffolds.[11,25] As the elastic modulus of cancellous bone ranges from 0.76 to 4.0

https://dx.doi.org/10.1021/acsomega.0c03127
ACS Omega 2020, 5, 22520−22528

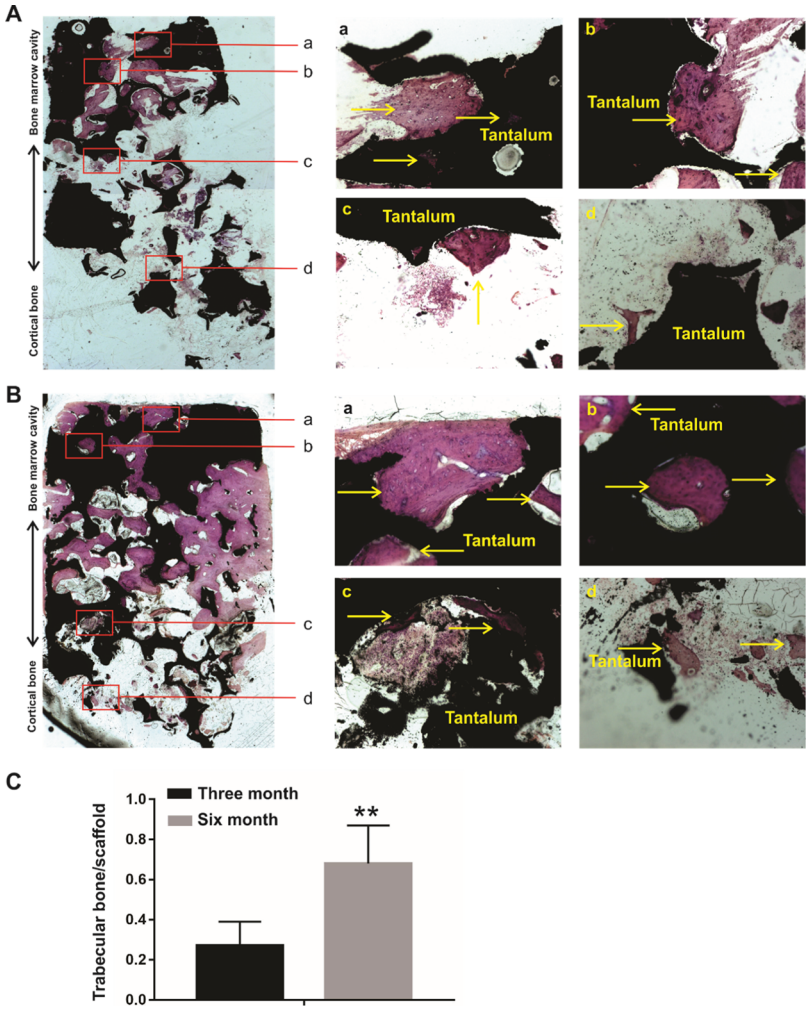

Figure 5. VG staining for retrieved tantalum rod-bone samples. (A) VG staining for retrieved tantalum rod-bone samples at 3 months after the implantation. A merged panoramic version in the left panel and distinct-separated images (a−d) are listed in the right panel, arrows indicated the new bone and tantalum rod interfaces. (B) VG staining for retrieved tantalum rod-bone samples at 6 months after the implantation. A merged panoramic version in the left panel and distinct-separated images (a−d) are listed in the right panel, arrows indicated the new bone and tantalum rod interfaces. (C) Quantitative analysis of new bone formation in 3 month and 6 month's specimens in VG staining. $^{**}p < 0.05$.

GPa, porosity of cancellous bone ranges from 75 to 90%, and pore size ranges from 50 to 300 μm.[25,31,32] Therefore, we designed our porous tantalum scaffold with the elastic modulus ranges from 0.5 to 4.0 GPa, porosity ranges from 60 to 80% and pore size ranges from 200 to 500 μm. All these parameters are approximate to cancellous bone. Different pore sizes influence different processes of bone ingrowth,[11,25,29−31] it was reported that larger than 300 μm pore size enhances vascularization, smaller than 150 μm pore size facilitates cell spanning across the pores, and larger than 200 μm pore size facilitates occupancy of the cells inside the pores. Besides pore size, the random and disorder distributed pattern is preferred for bone ingrowth. Hence, we designed the porous tantalum scaffold as a random distributed pore size range from 200 to 500 μm, which was proved to be conducive for bone ingrowth and host-implant integration. In addition, we found favorable bone ingrowth in the center of the scaffold, which proved that the random distributed pore size holds potential for continuous bone ingrowth.

Although porous tantalum has been clinically applied for interbody cervical fusions, reconstruction of large bony defects in primary and revision TKAs or THAs and so forth,[7,17−19] it is still conflicting as high porosity lowers the mechanical strength of the materials.[31] Thus, the balance between the microstructure and mechanical strength need to be achieved by regulating the porosity and pore size in order to achieve better in vivo performance. Through our in vivo assays, we found no gap formation between porous tantalum rod and host bone, porous tantalum and the host bone interfaces integrated with each other and new trabecular bone filled the pore of the porous tantalum material. The integration of porous tantalum and host bone was further confirmed by mechanical tests. We infer that the enough bone ingrowth may improve the mechanical strength of materials. These results indicated that the cancellous bone mimic scaffold may be suitable for the treatment of bone defect.

To determine the osteoinductivity of the porous tantalum scaffold, we inserted the porous tantalum rod in the center of bone marrow cavity. As the bone marrow cavity is a good source of MSCs, this model should also determine the osteoinductivity of the porous tantalum scaffold. As shown in Figures 4 and 5, new bone formation and ingrowth were found in the bone marrow cavity side of the porous tantalum rod, these results indicated that the porous tantalum scaffold is

https://dx.doi.org/10.1021/acsomega.0c03127
ACS Omega 2020, 5, 22520−22528

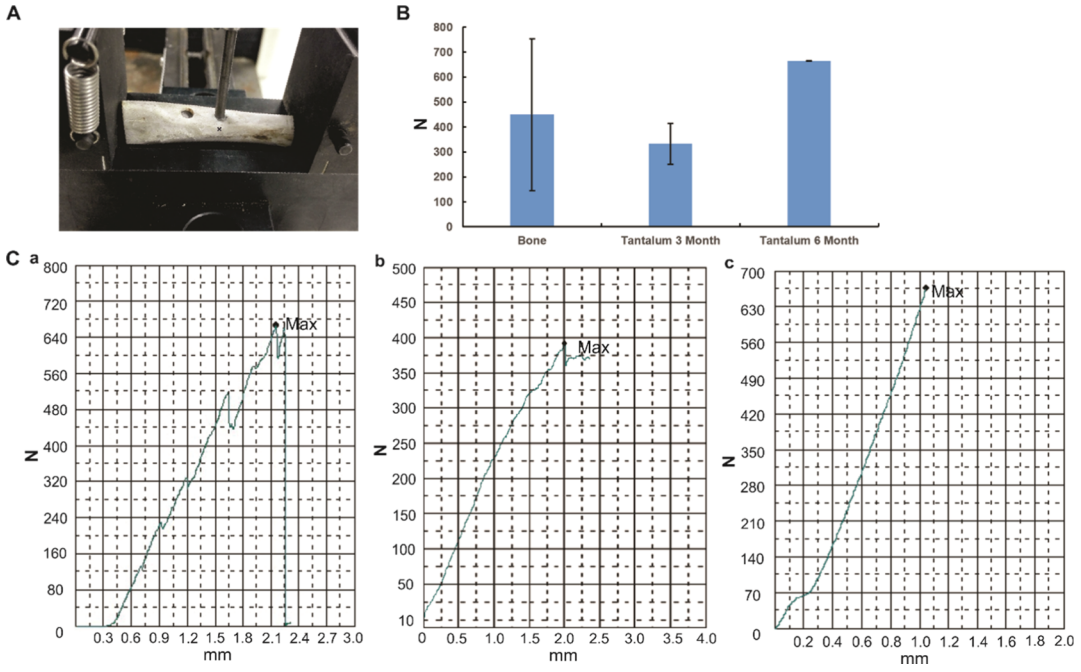

Figure 6. Push-out test for the evaluation of bone integration of the porous tantalum and host bone. (A) Universal testing machine for the push-out test. (B) Push-out strength in different samples, no statistical significance was found among groups. (C) Representative load-deformation curve for each group (a: normal bone, b: 3 month's specimen, c: 6 month's specimen).

osteoinductive. On the other hand, we found that more new bone formation in the bone marrow cavity side when compared with the cortical side we inferred that this was because instead of MSCs in the bone marrow side, osteocytes in the cortical side were limited in the formation of cancellous bone. In addition, porosity, pore diameter, and elastic modulus of cortical are different from cancellous bone,[11,25,32] although bone growth was also found in the cortical side of the tantalum rod (Figures 4 and 5), the porous tantalum scaffold is cancellous bone mimic, hence, density gradient and site specific scaffolds may be more helpful for the treatment of the clinical bone defect.

In the past decades, surgeons are interested in metal material-mediated bone defect repair; however, metal materials cause an electrochemical process known as corrosion which results in pain and makes it uncomfortable for patients.[7] Recently, tantalum, a bioinert metal was characterized to be extremely resistant to corrosion has been applied for clinical use.[7,14] In the present study, we designed a novel porous tantalum material, the cytotoxicity still needs to be evaluated. Through in vitro MTT assay, we found that the porous tantalum material is not toxic to MSCs. The in vivo pathological scoring also supported the safety of the porous tantalum (data not shown). That is to say, the novel porous tantalum scaffold is safe for implantation in vivo. Further research studies focus on long-term observation (longer than 1year) of bone ingrowth and compare with other porous materials should be carried out.

CONCLUSIONS

In summary, we manufactured a novel three-dimensional, multiscaled, and interconnected porous tantalum scaffold with porosity ranges from 60 to 80%, pore diameter ranges from 200 to 500 μm, elastic modulus ranges from 0.5 to 4.0 GPa, all the parameters are closer to trabecular bone. Through our in vitro and in vivo canine femoral shaft bone defect model, we found the novel porous tantalum scaffold is trabecular bone mimic, biocompatible, and osteoinductive, which holds potential for bone tissue engineering application.

MATERIALS AND METHODS

Manufacture and Structural Characterization of the Porous Tantalum Materials. The novel porous tantalum scaffold was manufactured by Chongqing Runze Pharmaceutical Co.,Ltd. (Chongqing, China). Briefly, pure tantalum powders were utilized for the manufacturing of porous tantalum materials. Tantalum powders with a specific amount of sponge carrier and additives, which were used to regulate the pore diameter of the porous scaffold, pore distribution, and porosity were subjected to slip-casting forming, then underwent 1500−2100 °C high temperature sintering, and finally approved to after treatment technology and necessary preparation (preparation procedures has been filed patents).

The porous tantalum was subjected to SEM (Nova NanoSEM, NE, USA accelerating voltage of 15 kV and JEOL SEM, Tokyo, Japan, accelerating voltage of 5 kV) analysis. The porous tantalum rod was also characterized using industrial CT (TOSCANER, Tokyo, Japan) at 500 Kv and 1.4 mA.

Cell Culture and Related Chemicals. The MSC cell line UC-MSCs (human umbilical cord-derived MSCs) was previously characterized.[33] The UC-MSC cell line was obtained from Chongqing Engineering Research Center of Stem Cell Therapy (Chongqing, China). The UC-MSCs were maintained in complete DMEM (Hyclone, China) containing 10% fetal bovine serum (Gibco, Australia), 100 units/mL penicillin, and 100 μg/mL streptomycin at 37 °C in 5% CO_2 incubator.

Culturing UC-MSCs on Tantalum Powder and SEM Analysis. The UC-MSCs were digested with trypsin and resuspended in culture medium at a concentration of 2×10^4/μL. Around 50 μL of cell suspension (10^6 cells) was seeded

https://dx.doi.org/10.1021/acsomega.0c03127
ACS Omega 2020, 5, 22520−22528

onto the porous tantalum powder (diameter 2−3 mm). The tantalum powders with cells were then incubated in an incubator for 2 h, and transferred into 6-well plates containing complete DMEM medium.

On day 3 and day 5, the UC-MSCs/tantalum powders were fixed in 2.5% glutaraldehyde buffered with 0.1 M sodiumcacodylate (NaC) solution at 4 °C overnight. Then, the samples were washed with 0.1 M NaC, and then subjected to secondary fixation with 1% osmium tetroxide in 0.1 M NaC for 2 h, followed by dehydrated in gradual ethanol boxes for 15 min, respectively, and finally subjected to SEM observation (HITACHI SU8010, Tokyo, Japan) with an accelerating voltage of 20 kV.

Cytotoxicity Examination. Novel porous tantalum scaffold extract preparation followed the ISO 10993-5, 2009 standard.[22] The extract was prepared according the principle of 'material weight/extraction transmitter = 0.2 g/mL', which was identified as 100% concentration. Briefly, sterile porous tantalum powders were maintained in complete DMEM and kept in a CO_2 incubator for 72 h. The extract was sterilized with the use of 0.22 μm filter.

As for the MTT assay, 200 μL of porous tantalum extract (experimental group) or complete DMEM (control group) were added in a 96-well plate, then UC-MSC cells were resuspended, and seeded at a concentration of 2×10^4 per well. At designed time points, 20 μL of MTT (5 mg/mL) medium was added to each well (pH 7.4) and the plate was incubated in a CO_2 incubator at 37 °C for 4 h, optical density value of each well was determined at a wavelength of 490 nm.

Construction of Canine Femoral Shaft Bone Defect Models and Implantation of Porous Tantalum Rod. All animal experiments were performed according to institutional guidelines under the approved protocols by the Chongqing Administration Rule of Laboratory Animals and the National Institutes of Health Guide for the Care and Use of Laboratory Animals. A total of 7 adult beagle dogs (weight 6−8 Kg) were selected. After intraperitoneal anesthesia with 3% pentobarbital sodium (1 mL/kg) and standard aseptic surgical procedures, the midpiece of the femur shaft was exposed by a lateral incision. A bone defect model was constructed with the use of a surgery drill bit at the middle part of the femur shaft, which resulted in a bone defect with a width of ∼4 mm and a depth of 8 mm (reach to the middle part of bone marrow cavity). A porous tantalum rod (4 mm in diameter and 8 mm in height) was implanted in the femur along with the defect, which was as close as possible in contact with the host bone. Each Canine Femur was implanted with two porous tantalum rods, and left thigh was selected as the surgical side. After the surgical procedures, the wound was sutured after adequate hemostasis. X-ray was taken after the surgery to confirm that the tantalum rods were in the femur shaft and without a peri-implant fracture. The animals were kept in independent cages with standard conditions.

At the indicated time points, animals were euthanized by overdose intraperitoneal pentobarbital sodium injection (Sigma-Aldrich, United States). All efforts were made to minimize the suffering of the animals, the animal was kept in standard conditions until it was confirmed that the animal was sacrificed. Then, the femurs were extracted to observe the bone growth around the porous tantalum rods. A hollow orthopaedic drill with a diameter of ∼5 mm was used to completely remove the porous tantalum rods.

Hard Tissue Slicing and Staining. All harvested specimens were fixed immediately with 4% phosphate-buffered paraformaldehyde. After gradient dehydration in ethanol solutions (60, 75, 88, 95, and 100%), infiltration, embedding in epoxy resin, and polymerization were performed. Then, a metal slicer was utilized to slice the specimens along the direction parallel to the longitudinal axis of the novel porous tantalum rods, a porous tantalum rod plane was fully exposed. After that the slices were polished to 90 μm in thickness. Finally, sections were subjected to methylene blue and VG staining, osteogenesis and bone ingrowth of the porous tantalum−bone interface were recorded by microscopy. ImageJ software was used for the quantitative analysis the new bone formation in 3 and 6 month's VG staining, the ratio of the trabecular bone and tantalum scaffold was calculated in 5 different fields, respectively.

Push-Out Test. To confirm the interfacial bond strength between the bone and the implant, the specimens were tested by a mechanical push-out test at the indicated time points using universal testing machine (Shimadzu AG-IS, Kyoto, Japan). In brief, samples were fixed on a support fixture with a central hole (4 mm in diameter). Then, the fixture was firmly fixed onto the machine platform. The load was carried out collinearly along the long axis of the implant with a 3.0 mm cylindrical plunger. The test began with a consistent displacement speed of 0.5 mm/min, the test stopped when the fracture or failure (max load: 900 N) of the interface was observed. The push-out test strength was recorded from the peak on the load-deformation curve. Normal femoral shaft specimens were used as the control, max load was calculated according to the normal specimens.

Statistical Analysis. Quantitative data were expressed as mean ± SD. SPSS 20.0 statistical software (IBM, Armonk, NY, USA) was applied for data analysis. One-way analysis of variance (ANOVA) or *t*-test was used to determine the statistical significance with a cut off of $p < 0.05$.

AUTHOR INFORMATION

Corresponding Authors

Junyi Liao − *Department of Orthopaedic Surgery, The First Affiliated Hospital of Chongqing Medical University, Chongqing 400016, China;* orcid.org/0000-0002-9212-7484; Phone: 86-23 89011222; Email: liaojunyi@cqmu.edu.cn; Fax: 86-23 89011211

Wei Huang − *Department of Orthopaedic Surgery, The First Affiliated Hospital of Chongqing Medical University, Chongqing 400016, China;* orcid.org/0000-0002-8894-0982; Phone: 86-23 89011222; Email: huangwei68@263.net; Fax: 86-23 89011211

Authors

Xiaoyu Wang − *Department of Orthopaedic Surgery, The First Affiliated Hospital of Chongqing Medical University, Chongqing 400016, China*

Zhenglin Zhu − *Department of Orthopaedic Surgery, The First Affiliated Hospital of Chongqing Medical University, Chongqing 400016, China*

Haozuo Xiao − *Department of Orthopaedic Surgery, The First Affiliated Hospital of Chongqing Medical University, Chongqing 400016, China*

Changqi Luo − *Department of Orthopaedic Surgery, The First Affiliated Hospital of Chongqing Medical University, Chongqing 400016, China*

https://dx.doi.org/10.1021/acsomega.0c03127
ACS Omega 2020, 5, 22520−22528

Xiaoji Luo − *Department of Orthopaedic Surgery, The First Affiliated Hospital of Chongqing Medical University, Chongqing 400016, China*

Furong Lv − *Department of Radiology, The First Affiliated Hospital of Chongqing Medical University, Chongqing 400016, China*

Complete contact information is available at: https://pubs.acs.org/10.1021/acsomega.0c03127

Author Contributions

W.H. and F.L. conceived and designed the experiments; X.W., J.L., H.X., Z.Z., and C.L. performed the experiments and collected the data; J.L., X.W., X.L., and W.H. analyzed the data; W.H., F.L., and J.L. contributed reagents/materials/analysis tools; J.L. and W.H. wrote the manuscript; all the authors read and approved the manuscript.

Notes

The authors declare no competing financial interest.

■ ACKNOWLEDGMENTS

We would like to thank Chongqing Runze Pharmaceutical Co., Ltd. (Chongqing, China) for the supply of porous tantalum material, Ministry of Education Key Laboratory of Child Development and Disorders, The Children's Hospital, Chongqing Medical University (Chongqing, China) for the supply of UC-MSCs. The reported work was supported by the National Natural Science Foundation of China (NSFC) (#81371972, #81572142 and #81972069). This project was also supported by Natural Science Foundation of Chongqing Science and Technology Commission (#cstc2018jcyjAX0088, #cstc2017zdcy-zdyf0437, #cstc2017shmsA0787 and #cstc2018jscx-mszd0557), Major Project of Chongqing Health and Family Planning Commission (#2015-1-12), Cultivating Program of The First Affiliated Hospital of Chongqing Medical University (#2018PYJJ-11), and Pre-NSFC research program of Chongqing Medical University. Funding sources were not involved in the study design, in the collection, analysis, and interpretation of data; in writing of the report; and in the decision to submit the paper for publication.

■ REFERENCES

(1) Nauth, A.; Schemitsch, E.; Norris, B.; Nollin, Z.; Watson, J. T. Critical-Size Bone Defects: Is There a Consensus for Diagnosis and Treatment? *J. Orthop. Trauma* **2018**, *32*, S7−S11.

(2) Hak, D. J. The use of osteoconductive bone graft substitutes in orthopaedic trauma. *J. Am. Acad. Orthop. Surg.* **2007**, *15*, 525−536.

(3) Tatara, A. M.; Mikos, A. G. Tissue Engineering in Orthopaedics. *J. Bone Joint Surg.* **2016**, *98*, 1132−1139.

(4) Black, C. R. M.; Goriainov, V.; Gibbs, D.; Kanczler, J.; Tare, R. S.; Oreffo, R. O. C. Bone Tissue Engineering. *Curr. Mol. Biol. Rep.* **2015**, *1*, 132−140.

(5) Wheeler, D. L.; Enneking, W. F. Allograft bone decreases in strength in vivo over time. *Clin. Orthop. Relat. Res.* **2005**, *435*, 36−42.

(6) Mankin, H. J.; Gebhardt, M. C.; Jennings, L. C.; Springfield, D. S.; Tomford, W. W. Long-term results of allograft replacement in the management of bone tumors. *Clin. Orthop. Relat. Res.* **1996**, *324*, 86−97.

(7) Mohandas, G.; Oskolkov, N.; McMahon, M. T.; Walczak, P.; Janowski, M. Porous tantalum and tantalum oxide nanoparticles for regenerative medicine. *Acta Neurobiol. Exp.* **2014**, *74*, 188−196.

(8) Li, Y.; Zhou, J.; Pavanram, P.; Leeflang, M. A.; Fockaert, L. I.; Pouran, B.; Tümer, N.; Schröder, K.-U.; Mol, J. M. C.; Weinans, H.; Jahr, H.; Zadpoor, A. A. Additively manufactured biodegradable porous magnesium. *Acta Biomater.* **2018**, *67*, 378−392.

(9) Barnett, S. L.; Mayer, R. R.; Gondusky, J. S.; Choi, L.; Patel, J. J.; Gorab, R. S. Use of stepped porous titanium metaphyseal sleeves for tibial defects in revision total knee arthroplasty: short term results. *J. Arthroplasty* **2014**, *29*, 1219−1224.

(10) Yazdimamaghani, M.; Razavi, M.; Vashaee, D.; Moharamzadeh, K.; Boccaccini, A. R.; Tayebi, L. Porous magnesium-based scaffolds for tissue engineering. *Mater. Sci. Eng. C* **2017**, *71*, 1253−1266.

(11) Alvarez, K.; Nakajima, H. Metallic Scaffolds for Bone Regeneration. *Materials* **2009**, *2*, 790−832.

(12) Jang, T.-S.; Jung, H.-D.; Kim, S.; Moon, B.-S.; Baek, J.; Park, C.; Song, J.; Kim, H.-E. Multiscale porous titanium surfaces via a two-step etching process for improved mechanical and biological performance. *Biomed. Mater.* **2017**, *12*, 025008.

(13) Ahmadi, S. M.; Hedayati, R.; Li, Y.; Lietaert, K.; Tümer, N.; Fatemi, A.; Rans, C. D.; Pouran, B.; Weinans, H.; Zadpoor, A. A. Fatigue performance of additively manufactured meta-biomaterials: The effects of topology and material type. *Acta Biomater.* **2018**, *65*, 292−304.

(14) Lee, J. W.; Wen, H. B.; Gubbi, P.; Romanos, G. E. New bone formation and trabecular bone microarchitecture of highly porous tantalum compared to titanium implant threads: A pilot canine study. *Clin. Oral Implants Res.* **2018**, *29*, 164−174.

(15) Wei, X.; Zhao, D.; Wang, B.; Wang, W.; Kang, K.; Xie, H.; Liu, B.; Zhang, X.; Zhang, J.; Yang, Z. Tantalum coating of porous carbon scaffold supplemented with autologous bone marrow stromal stem cells for bone regenerationin vitroandin vivo. *Exp. Biol. Med.* **2016**, *241*, 592−602.

(16) Wang, Q.; Qiao, Y.; Cheng, M.; Jiang, G.; He, G.; Chen, Y.; Zhang, X.; Liu, X. Tantalum implanted entangled porous titanium promotes surface osseointegration and bone ingrowth. *Sci. Rep.* **2016**, *6*, 26248.

(17) Ma, J.; Sun, W.; Gao, F.; Guo, W.; Wang, Y.; Li, Z. Porous Tantalum Implant in Treating Osteonecrosis of the Femoral Head: Still a Viable Option? *Sci. Rep.* **2016**, *6*, 28227.

(18) Frigg, A.; Dougall, H.; Boyd, S.; Nigg, B. Can porous tantalum be used to achieve ankle and subtalar arthrodesis?: a pilot study. *Clin. Orthop. Relat. Res.* **2010**, *468*, 209−216.

(19) Bencharit, S.; Byrd, W. C.; Altarawneh, S.; Hosseini, B.; Leong, A.; Reside, G.; Morelli, T.; Offenbacher, S. Development and applications of porous tantalum trabecular metal-enhanced titanium dental implants. *Clin. Implant Dent. Relat. Res.* **2014**, *16*, 817−826.

(20) Liu, Z. H.; Guo, W. S.; Li, Z. R.; Cheng, L. M.; Zhang, Q. D.; Yue, D. B.; Shi, Z. C.; Wang, B. L.; Sun, W.; Zhang, N. F. Porous tantalum rods for treating osteonecrosis of the femoral head. *Genet. Mol. Res.* **2014**, *13*, 8342−8352.

(21) Liu, G.; Wang, J.; Yang, S.; Xu, W.; Ye, S.; Xia, T. Effect of a porous tantalum rod on early and intermediate stages of necrosis of the femoral head. *Biomed. Mater.* **2010**, *5*, 065003.

(22) Wang, Q.; Zhang, H.; Li, Q.; Ye, L.; Gan, H.; Liu, Y.; Wang, H.; Wang, Z. Biocompatibility and osteogenic properties of porous tantalum. *Exp. Ther. Med.* **2015**, *9*, 780−786.

(23) Melancon, D.; Bagheri, Z. S.; Johnston, R. B.; Liu, L.; Tanzer, M.; Pasini, D. Mechanical characterization of structurally porous biomaterials built via additive manufacturing: experiments, predictive models, and design maps for load-bearing bone replacement implants. *Acta Biomater.* **2017**, *63*, 350−368.

(24) Bose, S.; Robertson, S. F.; Bandyopadhyay, A. Surface modification of biomaterials and biomedical devices using additive manufacturing. *Acta Biomater.* **2018**, *66*, 6−22.

(25) Kapat, K.; Srivas, P. K.; Rameshbabu, A. P.; Maity, P. P.; Jana, S.; Dutta, J.; Majumdar, P.; Chakrabarti, D.; Dhara, S. Influence of Porosity and Pore-Size Distribution in Ti6Al4 V Foam on Physicomechanical Properties, Osteogenesis, and Quantitative Validation of Bone Ingrowth by Micro-Computed Tomography. *ACS Appl. Mater. Interfaces* **2017**, *9*, 39235−39248.

(26) Yan, X.; Chen, Y. R.; Song, Y. F.; Yang, M.; Ye, J.; Zhou, G.; Yu, J. K. Scaffold-Based Gene Therapeutics for Osteochondral Tissue Engineering. *Front. Pharmacol.* **2019**, *10*, 1534.

(27) Saltz, A.; Kandalam, U. Mesenchymal stem cells and alginate microcarriers for craniofacial bone tissue engineering: A review. *J. Biomed. Mater. Res.* **2016**, *104*, 1276−1284.
(28) Van Bael, S.; Chai, Y. C.; Truscello, S.; Moesen, M.; Kerckhofs, G.; Van Oosterwyck, H.; Kruth, J.-P.; Schrooten, J. The effect of pore geometry on the in vitro biological behavior of human periosteum-derived cells seeded on selective laser-melted Ti6Al4V bone scaffolds. *Acta Biomater.* **2012**, *8*, 2824−2834.
(29) de Wild, M.; Zimmermann, S.; Rüegg, J.; Schumacher, R.; Fleischmann, T.; Ghayor, C.; Weber, F. E. Influence of Micro-architecture on Osteoconduction and Mechanics of Porous Titanium Scaffolds Generated by Selective Laser Melting. *3D Printing and Additive Manufacturing* **2016**, *3*, 142−151.
(30) Frosch, K.-H.; Barvencik, F.; Lohmann, C. H.; Viereck, V.; Siggelkow, H.; Breme, J.; Dresing, K.; Stürmer, K. M. Migration, matrix production and lamellar bone formation of human osteoblast-like cells in porous titanium implants. *Cells Tissues Organs* **2002**, *170*, 214−227.
(31) Karageorgiou, V.; Kaplan, D. Porosity of 3D biomaterial scaffolds and osteogenesis. *Biomaterials* **2005**, *26*, 5474−5491.
(32) Stolk, J.; Verdonschot, N.; Cristofolini, L.; Toni, A.; Huiskes, R. Finite element and experimental models of cemented hip joint reconstructions can produce similar bone and cement strains in pre-clinical tests. *J. Biomech.* **2002**, *35*, 499−510.
(33) Shu, Y.; Yang, C.; Ji, X.; Zhang, L.; Bi, Y.; Yang, K.; Gong, M.; Liu, X.; Guo, Q.; Su, Y.; Qu, X.; Nan, G.; Zhao, C.; Zeng, Z.; Yu, X.; Zhang, R.; Yan, S.; Lei, J.; Wu, K.; Wu, Y.; An, L.; Huang, S.; Gong, C.; Yuan, C.; Liu, W.; Huang, B.; Feng, Y.; Zhang, B.; Dai, Z.; Shen, Y.; Luo, W.; Wang, X.; Haydon, R. C.; Luu, H. H.; Reid, R. R.; Wolf, J. M.; Lee, M. J.; He, T.-C.; Li, Y. Reversibly immortalized human umbilical cord-derived mesenchymal stem cells (UC-MSCs) are responsive to BMP9-induced osteogenic and adipogenic differentiation. *J. Cell. Biochem.* **2018**, *119*, 8872−8886.

https://dx.doi.org/10.1021/acsomega.0c03127
ACS Omega 2020, 5, 22520−22528